Continuous sensing and parameter estimation with the boundary time-crystal

Albert Cabot,[1] Federico Carollo,[1] and Igor Lesanovsky[1,2,3]

[1] *Institut für Theoretische Physik, Eberhard Karls Universität Tübingen, Auf der Morgenstelle 14, 72076 Tübingen, Germany.*
[2] *School of Physics and Astronomy, University of Nottingham, Nottingham, NG7 2RD, UK.*
[3] *Centre for the Mathematics and Theoretical Physics of Quantum Non-Equilibrium Systems, University of Nottingham, Nottingham, NG7 2RD, UK*

A boundary time-crystal is a quantum many-body system whose dynamics is governed by the competition between coherent driving and collective dissipation. It is composed of N two-level systems and features a transition between a stationary phase and an oscillatory one. The fact that the system is open allows to continuously monitor its quantum trajectories and to analyze their dependence on parameter changes. This enables the realization of a sensing device whose performance we investigate as a function of the monitoring time T and of the system size N. We find that the best achievable sensitivity is proportional to $\sqrt{TN}$, i.e., it follows the standard quantum limit in time and Heisenberg scaling in the particle number. This theoretical scaling can be achieved in the oscillatory time-crystal phase and it is rooted in emergent quantum correlations. The main challenge is, however, to tap this capability in a measurement protocol that is experimentally feasible. We demonstrate that the standard quantum limit can be surpassed by cascading two time-crystals, where the quantum trajectories of one time-crystal are used as input for the other one.

Interacting nonequilibrium quantum systems can undergo spontaneous time-translation symmetry breaking. The phases associated with this phenomenon are called time-crystals [1–3] and can be observed both in driven Hamiltonian systems and in dissipative scenarios. In spite of a variety of possible mechanisms underlying their emergence, a common feature is the presence of asymptotic oscillations in some observable of the system [1–3]. Such oscillations either break a discrete time-symmetry, by displaying a period which is a multiple of the driving period [4–17], or a continuous time-symmetry [18–32], by approaching a limit cycle under time-independent driving [33]. The boundary time-crystal (BTC) is a paradigmatic example of (continuous) dissipative time-crystal [18]. It manifests in collective spin systems, in which the interplay between driving and dissipation leads to an oscillatory phase [18, 22]. Various time-crystal phases have been reported in open quantum systems [7–17, 19, 21, 23–28, 30–32], including recent experimental observations in atom-cavity setups [14, 34].

Dissipative time-crystals provide an example of collective phenomena in which dissipation plays a constructive role. This contrasts its more archetypal role in which dissipation simply destroys quantum correlations, hence being usually detrimental for, e.g., quantum metrology protocols [36, 37]. Alternative quantum metrology approaches try to harness nonequilibrium phenomena in order to enhance the sensitivity of parameter estimation [38]. For instance, this is the case of protocols exploiting dissipative phase transitions [38–46]. Another key idea is to exploit the information contained in the emissions of open quantum systems via continuous monitoring protocols [38, 47–54]. Bounds to the fundamental sensitivity achievable by these *continuous sensors* have been derived [55, 56]. In general, they are difficult to saturate with bare photocounting or homodyne detection protocols [cf. Protocol I in Fig. 1]. However, strategies have been developed in order to improve the sensitivity of continuous sensors [57–59], as the use of auxiliary systems [60, 61]. Connecting to the latter idea, Ref. [60] provides a general protocol based on cascading the output [62–64] of the sensor to a replica system that is continuously monitored [cf. Protocol II in Fig. 1], which may enable the saturation of the fundamental bound.

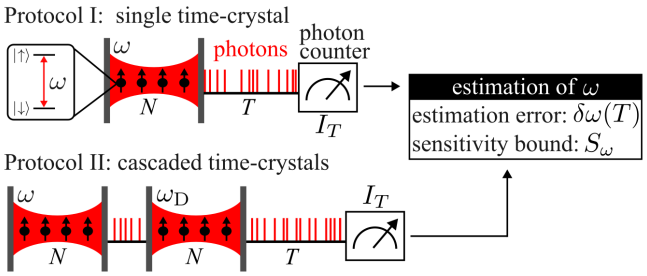

FIG. 1. **Continuous time-crystal sensor.** We consider N two-level systems subject to collective dissipation and driven with a Rabi frequency ω. This can be realized both with cavity [14, 34] or free space implementations [35]. We consider two sensing protocols, a single time-crystal (protocol I) and a two cascaded time-crystals (protocol II), where one system is driven with Rabi frequency ω and the other with ω_D. In both cases the parameter ω is estimated by measuring the photon output intensity I_T over a time interval of length T or in the stationary limit ($T \to \infty$). The estimation error $\delta\omega(T)$ — and whether it saturates the theoretical sensitivity bound S_ω — depends on the observation time and the protocol.

In this work we show how dissipative time-crystals can be exploited for sensing applications, reaching a sensitivity which can surpass the standard quantum limit. Recent works have studied BTCs from the perspective of critically enhanced sensing [44, 45], focusing on prop-

erties of the system alone, while Ref. [65] considered a discrete time-crystal for sensing time-dependent fields. Here, we instead assess the performance of BTCs as continuous sensors. The rationale is that time-crystal oscillations clearly manifest in the photocounting and homodyne detection signals even for finite sizes [66] and that this output is readily accessible in experiments. Firstly, we analyze the fundamental (theoretical) bound on the achievable sensitivity with these devices. Subsequently, we consider two different sensing protocols, based on photocounting experiments, see Fig. 1. Protocol I entails the direct monitoring of the signal while Protocol II relies on indirect monitoring of the photocurrent through a cascaded replica of the BTC, acting as a decoder, in the spirit of Ref. [60]. The time-crystal phase offers an enhanced sensitivity bound which scales linearly with the particle number N. This theoretical sensitivity cannot be achieved by Protocol I. Protocol II, on the other hand, allows to achieve the scaling $\sim N^{0.80}$, thus surpassing the standard quantum limit [38].

The model. – The BTC is composed of N spin-1/2 particles and described by the master equation ($\hbar = 1$)

$$\partial_t \hat{\rho} = -i\omega[\hat{S}_{\rm x}, \hat{\rho}] + \kappa \mathcal{D}[\hat{S}_-]\hat{\rho}\,, \tag{1}$$

with $\mathcal{D}[\hat{O}]\hat{\rho} = \hat{O}\hat{\rho}\hat{O}^\dagger - \{\hat{O}^\dagger\hat{O}, \hat{\rho}\}/2$ and $\hat{\rho}$ being the state of the system. We further defined $\hat{S}_\alpha = \frac{1}{2}\sum_{j=1}^{N}\hat{\sigma}_\alpha^{(j)}$ ($\alpha = {\rm x,y,z}$), with $\hat{\sigma}_\alpha^{(j)}$ being the Pauli matrices and $\hat{S}_\pm = \hat{S}_{\rm x} \pm i\hat{S}_{\rm y}$. Eq. (1) thus encodes collective spin decay with rate κ and a (resonant) driving with Rabi frequency ω. It preserves the total angular momentum, and we focus throughout on the fully symmetric sector. The above model was introduced in the context of cooperative resonance fluorescence, see, e.g., Refs. [67–70], and was recently recognized as a simple dissipative model displaying a time-crystal phase [18].

For collective systems such as that of Eq. (1), it is customary to rescale the collective decay rate κ by the system size in order to enforce a well-defined thermodynamic limit [22, 71]. However, we focus on finite-size systems and thus consider a N-independent rate, which further allows for a closer connection with experiments [35]. The system displays a stationary regime, characterized by fast relaxation to the stationary state, and an oscillatory regime, featuring long-lived oscillations [70]. The *quality factor* of the oscillations increases with system size [70] and diverges in the thermodynamic limit, where the system approaches the time-crystal phase [18, 22]. The two regimes are sharply separated by a critical Rabi frequency, $\omega_c = \kappa N/2$, as system size increases [70], the long-lived oscillations emerging for $\omega > \omega_c$.

Continuous sensing. – Our goal is to exploit the above system as a continuous sensor for estimating the Rabi frequency ω. To this end, we consider sensing protocols based on photocounting, so that the quantity that is measured is the time-integrated photon count or output intensity I_T up to a measurement time T. The latter is defined as $I_T = \frac{1}{T}\int_0^T dN(t)$, where $dN(t)$ is a random variable, taking the value 1 when a photon is detected at time t and 0 otherwise [72], with average value given by $\mathbb{E}[dN(t)] = \kappa dt {\rm Tr}[\hat{S}_+\hat{S}_-\hat{\rho}]$. Here, $\mathbb{E}[\cdot]$ represents the average over all possible realizations of the photocounting process [72]. A relevant figure of merit for the sensitivity of a protocol is the *estimation error*, or error propagation formula, which, for the above-introduced output intensity, reads

$$\delta\omega(T) = \sqrt{\mathbb{E}[I_T^2] - \mathbb{E}[I_T]^2}\left|\frac{\partial\mathbb{E}[I_T]}{\partial\omega}\right|^{-1}. \tag{2}$$

The first term on the right-hand side of the above equation is the standard deviation of the measurement, while the second one represents the susceptibility of the intensity on ω. In practice, the estimation error is the inverse of the signal to noise ratio. The *quantum Fisher information of the system and emission field* (QFI), $F_{\rm E}$, provides a lower bound for continuous sensing protocols [39],

$$\delta\omega(T) \geq [\sqrt{F_{\rm E}(\omega, T)}]^{-1}\,, \tag{3}$$

which applies to *any* protocol exploiting the information provided by the joint system and output state [39, 55, 60].

Here, we focus on a long measurement time limit, in which the system is described by its stationary state $\hat{\rho}_{\rm ss}$. Since I_T obeys a large deviation principle [73, 74], the time-integrated intensity tends to its mean [72], $\lim_{T\to\infty} I_T = \kappa{\rm Tr}[\hat{S}_+\hat{S}_-\hat{\rho}_{\rm ss}]$, and the standard deviation scales, away from phase transitions, as $\sqrt{(\mathbb{E}[I_T^2] - \mathbb{E}[I_T]^2)} \sim \overline{\sigma_{I_T}}/\sqrt{T}$. As a consequence, the estimation error asymptotically behaves as

$$\delta\omega \sim \frac{\overline{\delta\omega}}{\sqrt{T}}\,. \tag{4}$$

Both the prefactor for the standard deviation $\overline{\sigma_{I_T}}$ and the one for the estimation error $\overline{\delta\omega}$ are time-independent quantities (see also Supplemental Material [75]). The QFI scales linearly with time [55, 75], and thus

$$\sqrt{F_{\rm E}(\omega, T)} \sim \mathcal{S}_\omega\sqrt{T}\,. \tag{5}$$

The quantity $\mathcal{S}_\omega$ in the above equation is thus the (theoretical) *sensitivity bound* for the estimation, i.e., $(\overline{\delta\omega})^{-1} \leq \mathcal{S}_\omega$.

Fundamental bound on sensitivity. – In Fig. 2 we analyze the theoretically achievable bound on the sensitivity, S_ω. Deep inside the stationary phase this bound is constant, $\mathcal{S}_\omega \approx 2/\sqrt{\kappa}$, i.e., it does not depend on ω. This result is obtained via a Holstein-Primakoff approach (HP) (see [75]), which shows that spins organize in a large displaced state. Its fluctuations are annihilated by the dissipator and hence they do not contribute to the properties of the emitted light at leading order. The QFI is

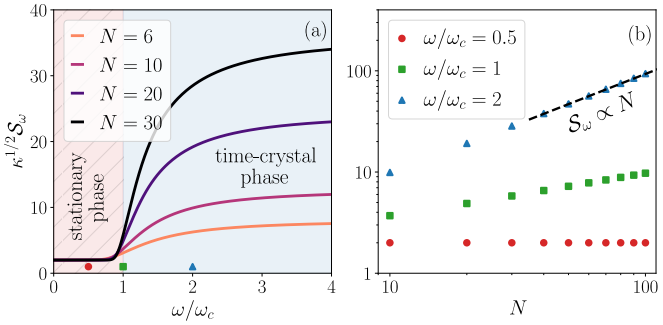

FIG. 2. **Sensitivity bound.** (a) Sensitivity bound $\mathcal{S}_\omega$ [cf. Eq. (5)], as a function of the Rabi frequency ω. (b) Sensitivity bound $\mathcal{S}_\omega$ as a function of the system size N for different values of the Rabi frequency. The black dashed line is a fit of the six points with largest size, yielding $\mathcal{S}_\omega \propto N^{1.0}$.

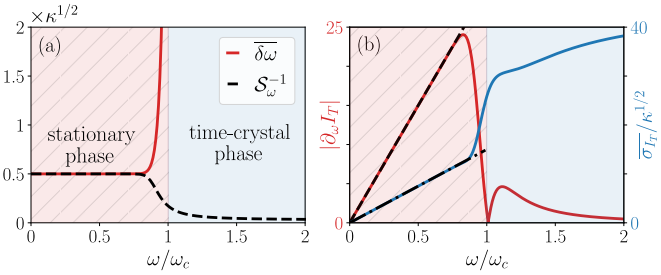

FIG. 3. **Protocol I.** (a) Red solid line: estimation error $\overline{\delta\omega}$ [cf. Eq. (4)], as a function of the Rabi frequency ω for $N = 30$. Black-dashed line: inverse sensitivity bound $\mathcal{S}_\omega^{-1}$ [Eq. (5)]. These quantities are plotted in units of $\sqrt{\kappa}$. (b) Left axis (red): absolute value of the derivative of the stationary intensity, as a function of the Rabi frequency. Right axis (blue): prefactor of the scaling of the standard deviation $\overline{\sigma_{I_T}}$, as a function of the Rabi frequency. Black broken lines correspond to analytical results for the stationary phase [75].

in this case dominated by the amplitude of the coherent displacement.

In the vicinity of ω_c we observe a sharp crossover with the sensitivity bound becoming larger in the oscillatory phase ($\omega/\omega_c > 1$). This feature becomes more and more pronounced the larger the system size. The sensitivity in the time-crystal phase indeed grows linearly, $\mathcal{S}_\omega \propto N$ [see Fig. 2(b)], well into the time-crystal regime (while at criticality the scaling is sublinear). From Fig. 2(a) it is also clear that for fixed system size N the sensitivity bound saturates upon increasing ω/ω_c. This shows that increasing the system size and increasing the Rabi frequency *do not* have the same effect on the sensitivity. Therefore, the N-dependency of the bound in the time-crystal phase is a genuine many-body effect. Notice that $\mathcal{S}_\omega \propto N$ corresponds to a N^2-scaling for the QFI, meaning that the time-crystal phase theoretically offers a Heisenberg limited sensitivity in the number of particles [38].

The system size enhancement of the sensitivity can be understood from the properties of the emergent many-body oscillations. As shown in Ref. [66], these oscillations translate directly into the photocounting signal, manifesting as an oscillatory detection signal. Increasing system size with fixed ω/ω_c has a twofold effect. First, the quality factor of the oscillations increases linearly with N [20, 22, 70], and thus the oscillations in the emitted field have an increasingly better defined frequency. Second, the amplitude of the oscillations also increases with system size (as more atoms emit synchronously), and thus the signal stands out more clearly from background noise [66]. The combination of these effects creates stronger correlations between the system and the emitted field, which are a known source for enhancement of the QFI [39, 55, 60]. An indirect signature of such strong correlations is the fact that the reduced state of the system in the time-crystal phase is close to the maximally mixed state [66, 76], which witnesses that the total state of system and emission field is highly correlated. Interestingly, the monitored state of the system in the time-crystal phase also displays multipartite entanglement [77]. In the following, we explore whether sensitivities close to the bound can be achieved using sensing protocols based on photocounting.

Protocol I. – The first protocol we consider is based on counting the number of emitted photons in a time window T. For long measurement times, a single (ideal) measurement run yields the stationary state intensity, while its standard deviation can be systematically studied using large deviations [75]. In Fig. 3(a) we present the estimation error for this protocol. The smallest estimation errors are attained in the stationary phase. Indeed at the transition the estimation error increases steeply and in the time-crystal phase it assumes values which are much larger than the bound S_ω. The "bad" performance under this measurement protocol can be understood from the data shown in Fig. 3(b). There we observe that in the time-crystal phase the derivative of the intensity with ω diminishes significantly while the standard deviation displays the opposite trend.

Interestingly, simple photocounting saturates the sensitivity bound in the stationary phase. This can be understood by applying the HP approximation to methods from large deviation theory, which allows us to obtain an analytical approximation for the error [75]: $\overline{\delta\omega} \approx 0.5\sqrt{\kappa}$. This value agrees with the numerical results of Fig. 3(b) (see black-broken lines). The physical interpretation is the same as for the QFI, i.e., to leading order the emitted light displays the same properties as a state with large coherent amplitude.

Protocol II. – In the second protocol, inspired by Ref. [60], the emission of the system of interest, the *sensor*, is cascaded [62, 63] into an auxiliary system with same degrees of freedom, referred to as *decoder* (see Fig. 1). This protocol builds on the emergence of dark states in the cascaded system, a situation explored in de-

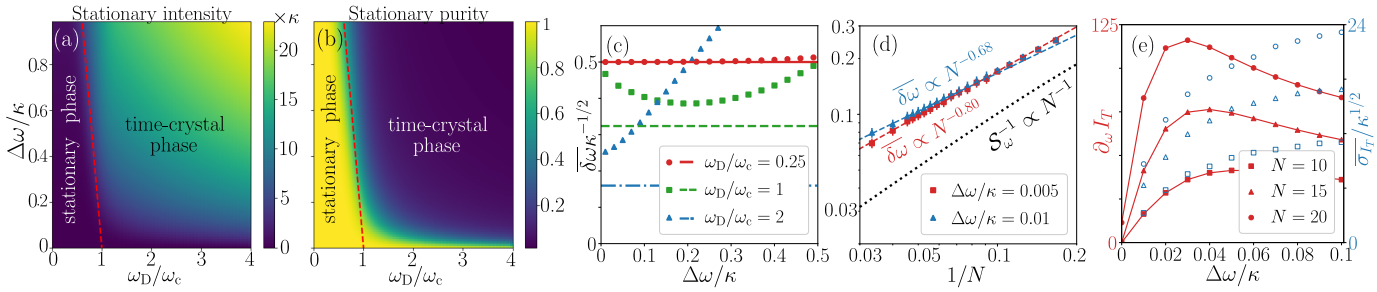

FIG. 4. **Protocol II.** (a) Stationary intensity of the cascaded system varying $\Delta\omega = \omega - \omega_D$ and ω_D. At the line $\Delta\omega = 0$ the emitted intensity is zero. This quantity is plotted in units of κ. (b) Purity of the stationary state of the cascaded system. In panels (a), (b) the red dashed line corresponds to the mean-field transition line. In both cases $N = 10$. (c) Estimation error $\overline{\delta\omega}$ [cf. Eq. (4)] varying the Rabi frequency difference between the spin systems $\Delta\omega$, and for three different points in the phase diagram. Color lines correspond to the inverse of the sensitivity bound $\mathcal{S}_\omega^{-1}$ [cf. Eq. (5)] displayed in Fig. 2(a). In this panel we have considered $N = 6$. (d) Color points: estimation error $\overline{\delta\omega}$ varying system size $N \in [6, 30]$ for $\omega_D/\omega_c = 2$. The black dotted line corresponds to the sensitivity bound $\mathcal{S}_\omega^{-1}$ displayed in Fig. 2(b). The color dashed lines correspond to fits for the eight data points with largest size, yielding the exponential laws depicted in the figure (see [75] for more details). (e) Left (red) axis: derivative of the (stationary) emitted intensity with respect to ω as a function of $\Delta\omega$. Right (blue) axis: prefactor for the standard deviation of the output intensity, as a function of $\Delta\omega$. In this panel $\omega_D/\omega_c = 2$.

tail in Ref. [64]. Optimal sensing is then achieved close to the parameters in which the dark state is present [60]. We consider two BTCs in cascaded configuration: all output light of the sensor (system 1) is fed into the decoder (system 2), while no light of decoder returns to the sensor [62–64]. Protocol II is described by the master equation:

$$\partial_t\hat{\rho} = -i[\omega\hat{S}_x^{(1)} + \omega_D\hat{S}_x^{(2)} + \hat{H}_c, \hat{\rho}] + \kappa\mathcal{D}[\hat{J}_-]\hat{\rho}. \qquad (6)$$

where $\hat{H}_c = -i\kappa(\hat{S}_+^{(2)}\hat{S}_-^{(1)} - \hat{S}_+^{(1)}\hat{S}_-^{(2)})/2$ and $\hat{J}_\alpha = \hat{S}_\alpha^{(1)} + \hat{S}_\alpha^{(2)}$ are the total angular momentum operators. Here, $\hat{S}_\alpha^{(1,2)}$ are macroscopic spin operators, each one associated with N two-level systems.

Before analyzing the sensitivity of the second protocol we briefly summarize the most important features of the cascaded dynamical system. A crucial result is that the stationary state of Eq. (6) is a dark state — for any ratio ω/κ — as long as $\omega_D = \omega$ (see [75] for its analytical expression). Interestingly, well into the stationary phase, it is separable, while for $\omega/\kappa \gg 1$ it tends to the highly correlated singlet state of the total angular momentum. Once we break the condition $\Delta\omega = \omega - \omega_D = 0$, the cascaded system emits light. In Fig. 4(a) we show its stationary emission intensity: $\lim_{T\to\infty} I_T = \kappa\mathrm{Tr}[\hat{J}_+\hat{J}_-\hat{\rho}_{ss}]$. For $\omega_D/\omega_c > 1$ and $\Delta\omega > 0$, the system emits much more intensely than for $\omega_D/\omega_c < 1$. Looking at the purity of the stationary state [Fig. 4(b)], it is possible to see a clear separation between these two regions, the brighter one being highly mixed, while the darker one displaying an almost pure stationary state. Notice that the reduced state of the sensor is exactly the same as for Eq. (1) [64]. Hence, the mixed bright phase corresponds to the sensor being in the time-crystal phase, while the pure phase corresponds to the sensor being stationary. Using the HP approximation [75], we find that the stationary phase is assumed when $\omega, \omega_D < \omega_c$ and $\Delta\omega < (\omega_c - \omega_D)/2$. This result is accurate even for small sizes [see red-dashed line in Fig. 4(a-b)]. In this phase, each collective spin organizes itself in a coherent state with large amplitude plus Gaussian bosonic fluctuations. Their stationary state is a two mode separable state, in which each mode displays analogous properties [75].

We proceed by analyzing the sensitivity of Protocol II, which estimates ω from the output intensity of the cascaded system [see Fig. 1]. In Fig. 4(c) we provide the estimation error as function of $\Delta\omega$ for different points of the phase diagram. A first observation is that in the stationary phase there is no improvement with respect to Protocol I. This can be understood again via HP in combination with methods from large deviations (see [75]) which predicts the estimation error to be: $\overline{\delta\omega} \approx 0.5\sqrt{\kappa}$. The physical interpretation of this result is the same as for the individual system: the emitted light has essentially the same properties as a coherent state. In contrast, in the cascaded time-crystal phase the sensitivity increases. The estimation error is smaller than in the stationary phase and it improves further with increasing system size, as shown in Fig. 4(c-d). In panel (d) we analyze the system size dependence considering two values of $\Delta\omega$ close to the dark state condition. By fitting the points for the largest system sizes N (dashed lines), we obtain $\overline{\delta\omega} \propto N^{-\alpha}$. The exponents are $\alpha = 0.68$ for $\Delta\omega/\kappa = 0.01$ and $\alpha = 0.80$ for $\Delta\omega/\kappa = 0.005$. The sensitivity thus surpasses the standard quantum limit in the number of particles. For large system sizes the system performs better closer to the dark state point $\Delta\omega = 0$. The estimation error displays a non-monotonous behavior with respect to $\Delta\omega$, which reflects the presence of an optimal value for $\overline{\delta\omega}$. This can be understood by analyzing separately the two quantities that contribute to the

estimation error [see Fig. 4(e)]: as system size increases, the derivative of the stationary intensity develops an increasingly sharper peak closer to zero. In contrast, the (time rescaled) standard deviation of the intensity increases monotonously with system size and $\Delta\omega$. The interplay of these two effects makes the optimal estimation error to be found for an intermediate $\Delta\omega$ that depends on N.

Conclusions. – We have investigated parameter estimation through continuously monitoring quantum trajectories of a BTC. We have shown that the time-crystal phase in principle offers enhanced sensitivity, which manifests through the Heisenberg scaling of the QFI ($\propto N^2$) in the number of particles, N. Investigating two protocols, we have shown that a sensitivity surpassing the standard quantum limit can indeed be practically achieved in a cascaded setup of two time-crystals. In view of recent experiments [35], it would be interesting to consider other continuous monitoring protocols, such as homodyne detection and/or to include finite detection efficiency. Finally, in the presence of local decay, we expect the observed phenomena to persist and become more robust as the number of atoms increases due to the increasingly large separation of timescales between collective and local processes [75].

Acknowledgements. – We are grateful for financing from the Baden-Württemberg Stiftung through Project No. BWST_ISF2019-23. We also acknowledge funding from the Deutsche Forschungsgemeinschaft (DFG, German Research Foundation) under Project No. 435696605 and through the Research Unit FOR 5413/1, Grant No. 465199066. This project has also received funding from the European Union's Horizon Europe research and innovation program under Grant Agreement No. 101046968 (BRISQ). F.C. is indebted to the Baden-Württemberg Stiftung for the financial support by the Eliteprogramme for Postdocs. We acknowledge the use of Qutip python library [78, 79]. We acknowledge support by the state of Baden-Württemberg through bwHPC and the German Research Foundation (DFG) through grant no INST 40/575-1 FUGG (JUSTUS 2 cluster).

[1] K. Sacha and J. Zakrzewski, Rep. Prog. Phys. **81**, 016401 (2017).
[2] D. V. Else, C. Monroe, C. Nayak, and N. Y. Yao, Annu. Rev. Condens. Matter Phys. **11**, 467 (2020).
[3] M. P. Zaletel, M. Lukin, C. Monroe, C. Nayak, F. Wilczek, and N. Y. Yao, Rev. Mod. Phys. **95**, 031001 (2023).
[4] D. V. Else, B. Bauer, and C. Nayak, Phys. Rev. Lett. **117**, 090402 (2016).
[5] V. Khemani, A. Lazarides, R. Moessner, and S. L. Sondhi, Phys. Rev. Lett. **116**, 250401 (2016).
[6] N. Y. Yao, A. C. Potter, I.-D. Potirniche, and A. Vishwanath, Phys. Rev. Lett. **118**, 030401 (2017).
[7] Z. Gong, R. Hamazaki, and M. Ueda, Phys. Rev. Lett. **120**, 040404 (2018).
[8] R. R. W. Wang, B. Xing, G. G. Carlo, and D. Poletti, Phys. Rev. E **97**, 020202 (2018).
[9] F. M. Gambetta, F. Carollo, M. Marcuzzi, J. P. Garrahan, and I. Lesanovsky, Phys. Rev. Lett. **122**, 015701 (2019).
[10] A. Lazarides, S. Roy, F. Piazza, and R. Moessner, Phys. Rev. Research **2**, 022002 (2020).
[11] A. Riera-Campeny, M. Moreno-Cardoner, and A. Sanpera, Quantum **4**, 270 (2020).
[12] B. Zhu, J. Marino, N. Y. Yao, M. D. Lukin, and E. A. Demler, New J. Phys. **21**, 073028 (2019).
[13] K. Chinzei and T. N. Ikeda, Phys. Rev. Lett. **125**, 060601 (2020).
[14] H. Keßler, P. Kongkhambut, C. Georges, L. Mathey, J. G. Cosme, and A. Hemmerich, Phys. Rev. Lett. **127**, 043602 (2021).
[15] R. J. L. Tuquero, J. Skulte, L. Mathey, and J. G. Cosme, Phys. Rev. A **105**, 043311 (2022).
[16] S. Sarkar and Y. Dubi, Comm. Phys. **5**, 1 (2022).
[17] A. Cabot, F. Carollo, and I. Lesanovsky, Phys. Rev. B **106**, 134311 (2022).
[18] F. Iemini, A. Russomanno, J. Keeling, M. Schirò, M. Dalmonte, and R. Fazio, Phys. Rev. Lett. **121**, 035301 (2018).
[19] K. Tucker, B. Zhu, R. J. Lewis-Swan, J. Marino, F. Jimenez, J. G. Restrepo, and A. M. Rey, New J. Phys. **20**, 123003 (2018).
[20] G. Buonaiuto, F. Carollo, B. Olmos, and I. Lesanovsky, Phys. Rev. Lett. **127**, 133601 (2021).
[21] C. Lledó and M. H. Szymańska, New J. Phys. **22**, 075002 (2020).
[22] F. Carollo and I. Lesanovsky, Phys. Rev. A **105**, L040202 (2022).
[23] K. Seibold, R. Rota, and V. Savona, Phys. Rev. A **101**, 033839 (2020).
[24] B. Buča and D. Jaksch, Phys. Rev. Lett. **123**, 260401 (2019).
[25] B. Buča, J. Tindall, and D. Jaksch, Nat. Commun. **10**, 1 (2019).
[26] C. Booker, B. Buča, and D. Jaksch, New J. Phys. **22**, 085007 (2020).
[27] L. F. d. Prazeres, L. d. S. Souza, and F. Iemini, Phys. Rev. B **103**, 184308 (2021).
[28] G. Piccitto, M. Wauters, F. Nori, and N. Shammah, Phys. Rev. B **104**, 014307 (2021).
[29] A. C. Lourenço, L. F. d. Prazeres, T. O. Maciel, F. Iemini, and E. I. Duzzioni, Phys. Rev. B **105**, 134422 (2022).
[30] M. Hajdušek, P. Solanki, R. Fazio, and S. Vinjanampathy, Phys. Rev. Lett. **128**, 080603 (2022).
[31] M. Krishna, P. Solanki, M. Hajdušek, and S. Vinjanampathy, Phys. Rev. Lett. **130**, 150401 (2023).
[32] R. Mattes, I. Lesanovsky, and F. Carollo, arXiv preprint arXiv:2303.07725 (2023).
[33] S. H. Strogatz, *Nonlinear dynamics and chaos: with applications to physics, biology, chemistry, and engineering* (CRC press, 2018).
[34] P. Kongkhambut, J. Skulte, L. Mathey, J. G. Cosme, A. Hemmerich, and H. Keßler, Science **377**, 670 (2022).
[35] G. Ferioli, A. Glicenstein, I. Ferrier-Barbut, and A. Browaeys, Nature Physics , 1 (2023).
[36] C. L. Degen, F. Reinhard, and P. Cappellaro, Rev. Mod. Phys. **89**, 035002 (2017).

[37] D. Braun, G. Adesso, F. Benatti, R. Floreanini, U. Marzolino, M. W. Mitchell, and S. Pirandola, Rev. Mod. Phys. **90**, 035006 (2018).
[38] T. Ilias, D. Yang, S. F. Huelga, and M. B. Plenio, PRX Quantum **3**, 010354 (2022).
[39] K. Macieszczak, M. Guţă, I. Lesanovsky, and J. P. Garrahan, Phys. Rev. A **93**, 022103 (2016).
[40] S. Fernández-Lorenzo and D. Porras, Phys. Rev. A **96**, 013817 (2017).
[41] T. L. Heugel, M. Biondi, O. Zilberberg, and R. Chitra, Phys. Rev. Lett. **123**, 173601 (2019).
[42] L. Garbe, M. Bina, A. Keller, M. G. A. Paris, and S. Felicetti, Phys. Rev. Lett. **124**, 120504 (2020).
[43] R. Di Candia, F. Minganti, K. Petrovnin, G. Paraoanu, and S. Felicetti, npj Quantum Information **9**, 23 (2023).
[44] V. P. Pavlov, D. Porras, and P. A. Ivanov, Physica Scripta **98**, 095103 (2023).
[45] V. Montenegro, M. G. Genoni, A. Bayat, and M. G. Paris, Communications Physics **6**, 304 (2023).
[46] T. Ilias, D. Yang, S. F. Huelga, and M. B. Plenio, arXiv preprint arXiv:2304.02050 (2023).
[47] J. Gambetta and H. M. Wiseman, Phys. Rev. A **64**, 042105 (2001).
[48] A. H. Kiilerich and K. Mølmer, Phys. Rev. A **89**, 052110 (2014).
[49] F. Albarelli, M. A. C. Rossi, M. G. A. Paris, and M. G. Genoni, New J. Phys. **19**, 123011 (2017).
[50] F. Albarelli, M. A. C. Rossi, D. Tamascelli, and M. G. Genoni, Quantum **2**, 110 (2018).
[51] A. Shankar, G. P. Greve, B. Wu, J. K. Thompson, and M. Holland, Phys. Rev. Lett. **122**, 233602 (2019).
[52] F. Albarelli, M. A. C. Rossi, and M. G. Genoni, Int. J. Quantum Inf. **18**, 1941013 (2020).
[53] M. A. C. Rossi, F. Albarelli, D. Tamascelli, and M. G. Genoni, Phys. Rev. Lett. **125**, 200505 (2020).
[54] H. I. Nurdin and M. Guţă, Annu. Rev. Control **54**, 295 (2022).
[55] S. Gammelmark and K. Mølmer, Phys. Rev. Lett. **112**, 170401 (2014).
[56] C. Catana, L. Bouten, and M. Guţă, J. Phys. A Math. Theor. **48**, 365301 (2015).
[57] S. Gammelmark and K. Mølmer, Phys. Rev. A **87**, 032115 (2013).
[58] A. H. Kiilerich and K. Mølmer, Phys. Rev. A **94**, 032103 (2016).
[59] A. Fallani, M. A. C. Rossi, D. Tamascelli, and M. G. Genoni, PRX Quantum **3**, 020310 (2022).
[60] D. Yang, S. F. Huelga, and M. B. Plenio, Phys. Rev. X **13**, 031012 (2023).
[61] A. Godley and M. Guta, Quantum **7**, 973 (2023).
[62] C. W. Gardiner, Phys. Rev. Lett. **70**, 2269 (1993).
[63] H. J. Carmichael, Phys. Rev. Lett. **70**, 2273 (1993).
[64] K. Stannigel, P. Rabl, and P. Zoller, New J. Phys. **14**, 063014 (2012).
[65] F. Iemini, R. Fazio, and A. Sanpera, arXiv preprint arXiv:2306.03927 (2023).
[66] A. Cabot, L. S. Muhle, F. Carollo, and I. Lesanovsky, Phys. Rev. A **108**, L041303 (2023).
[67] G. S. Agarwal, A. C. Brown, L. M. Narducci, and G. Vetri, Phys. Rev. A **15**, 1613 (1977).
[68] L. M. Narducci, D. H. Feng, R. Gilmore, and G. S. Agarwal, Phys. Rev. A **18**, 1571 (1978).
[69] P. Drummond and H. Carmichael, Opt. Commun. **27**, 160 (1978).
[70] H. J. Carmichael, J. Phys. B At. Mol. Opt. **13**, 3551 (1980).
[71] F. Benatti, F. Carollo, R. Floreanini, and H. Narnhofer, J. Phys. A: Math. Theor. **51**, 325001 (2018).
[72] H. M. Wiseman and G. J. Milburn, *Quantum measurement and control* (Cambridge university press, 2009).
[73] J. P. Garrahan and I. Lesanovsky, Phys. Rev. Lett. **104**, 160601 (2010).
[74] F. Carollo, J. P. Garrahan, I. Lesanovsky, and C. Pérez-Espigares, Phys. Rev. A **98**, 010103 (2018).
[75] See the Supplemental Material for details, which includes Refs. [80, 81].
[76] J. Hannukainen and J. Larson, Phys. Rev. A **98**, 042113 (2018).
[77] G. Passarelli, X. Turkeshi, A. Russomanno, P. Lucignano, M. Schirò, and R. Fazio, arXiv preprint arXiv:2306.00841 (2023).
[78] J. Johansson, P. Nation, and F. Nori, Comput. Phys. Commun. **183**, 1760 (2012).
[79] J. Johansson, P. Nation, and F. Nori, Comput. Phys. Commun. **184**, 1234 (2013).
[80] E. M. Kessler, G. Giedke, A. Imamoglu, S. F. Yelin, M. D. Lukin, and J. I. Cirac, Phys. Rev. A **86**, 012116 (2012).
[81] K. Macieszczak, M. Guţă, I. Lesanovsky, and J. P. Garrahan, Phys. Rev. Lett. **116**, 240404 (2016).